

An “X-ray Dim Isolated Neutron Star” in Binary?

JIE LIN,^{1,2,3} CHUNQIAN LI,⁴ WEIYANG WANG,^{1,2,3} HENG XU,⁵ JINCHEN JIANG,⁵ DAOYE YANG,⁴ SHAHIDIN YAQUP,⁶
ABDUSAMATJAN ISKANDA,⁶ SHUGUO MA,⁶ HUBIAO NIU,⁶ ALI ESAMDIN,⁶ GAVIN RAMSAY,⁷ JOSE I. VINES,⁸
JIANRONG SHI,^{4,9} AND RENXIN XU^{1,2,3}

¹*Department of Astronomy, Peking University, Beijing 100871, People’s Republic of China*

²*State Key Laboratory of Nuclear Physics and Technology, School of Physics, Peking University, Beijing 100871, People’s Republic of China*

³*Kavli Institute for Astronomy and Astrophysics, Peking University, Beijing 100871, People’s Republic of China*

⁴*CAS Key Laboratory of Optical Astronomy, National Astronomical Observatories, Chinese Academy of Sciences, Beijing 100101, People’s Republic of China*

⁵*National Astronomical Observatories, Chinese Academy of Sciences, Beijing 100101, People’s Republic of China*

⁶*XinJiang Astronomical Observatory, Chinese Academy of Sciences*

⁷*Armagh Observatory and Planetarium, College Hill, Armagh BT61 9DG, UK*

⁸*Departamento de Astronomía, Universidad de Chile, Casilla 36-D, Santiago, Chile*

⁹*School of Astronomy and Space Science, University of Chinese Academy of Sciences, Beijing 100049, People’s Republic of China*

ABSTRACT

We report the discovery of a dark companion to 2MASS J15274848+3536572 with an orbital period of 6.14 hours. Combining the radial velocity of LAMOST observation and the modelling of the multi-band light curve, one has a mass function of $\simeq 0.135 M_{\odot}$, an inclination of $43.94^{+0.33}_{-0.21}^{\circ}$, and a mass ratio of $0.58^{+0.048}_{-0.018}$, which demonstrate the binary nature of a dark companion with mass of $1.01 \pm 0.08 M_{\odot}$ and a main-sequence K star of $0.59 \pm 0.05 M_{\odot}$. LAMOST optical spectra at a range of orbital phase reveals extra peaked H $_{\alpha}$ emission that suggests the presence of an accretion disk. The dark companion does not seem to be a white dwarf because the lack of any observed dwarf nova outbursts contradicts with the disk instability model in long-term data archive. Alternatively, we propose a scenario that the dark companion is a neutron star, but we have not detected radio pulsation or single pulse from the system with the FAST (Five-hundred-meter Aperture Spherical radio Telescope), which hints a radio quiet compact object. If the dark companion is identified as a neutron star, it will be nearest (~ 118 pc) and lightest neutron star. Furthermore, a kinematic analysis of the system’s orbit in the Galaxy may suggest its supernova event is associated with the radionuclide ^{60}Fe signal observed from the deep-sea crusts. This radio-quiet and X-ray dim nearby neutron star may resemble an XDINS (X-ray dim isolated neutron star), but in a binary.

Keywords: binaries:spectroscopic — stars:neutron star — stars:individual:2MASS J15274848+3536572

1. INTRODUCTION

The puzzling equation of state of dense matter inside neutron stars (NSs) is focused in both microphysics and astrophysics, and moreover, the diversity of NS’s manifestations challenges a simple belief about their astronomical origins (e.g., [Kaspi 2010](#)). Among the populations in the NS zoo, there is a small group called X-ray dim isolated neutron stars (XDINSs), characterized by low thermal X-ray luminosity in the neighbourhood. Is there any XDINS-like compact object in binary? How can one find it? This is the focus of the present work.

Corresponding author: Renxin Xu
r.x.xu@pku.edu.cn

Corresponding author: Jianrong Shi
sjr@nao.cas.cn

Up-to-now, only seven XDINSs were discovered by the ROSAT all-sky observations, which are nicknamed as the Magnificent Seven (Voges et al. 1996). An intriguing feature, that is, they are characterized by Planck-like spectra in X-ray bands as well as in optical bands but with an ordered excess, and non-detection of radio signals (Haberl 2007). XDINSs are peculiar objects to reveal the equation of state (EOS) at supranuclear density and offer an unprecedented opportunity to study atmospheric emission on the surface (e.g., Ho et al. 2007; Wang et al. 2017, 2018). If similar objects can be discovered outside our local volume, it will be significant for understanding their properties as a group and relationship to other galactic isolated neutron star (INS) families. A promising INS candidate was found from the 2XMMp catalogue of serendipitous sources (Pires et al. 2009), and then four newly discovered INS (isolated neutron star) candidates were reported from the 4XMM-DR10 catalogue (Rigoselli et al. 2022). Such stars are measured to be close from us ($\sim 120 - 500$ pc), and as numerous as young radio and γ -ray pulsars locally, suggesting that there may be lots of similar Galactic sources still unknown.

We focus on the binary systems with compact objects, which can provide an opportunity to develop the accretion disk model, and test the prediction of binary interaction theories (Mukai 2017; Langer 2012). Interestingly, neutron stars with the XDINS-like characters, which is of great interest in the EOS problem, have not been found in binaries yet (e.g., Pires et al. 2015). In addition, the discovery and observed mass distributions of NSs and black holes (BHs) in the Milky Way is crucial for understanding core collapse supernovae and the evolution of massive stars (Fryer et al. 2012; Woosley et al. 2020). So far, most compact binaries with neutron star, or black hole are identified from the radio, X-ray, and gamma-ray surveys, and from the gravitational wave. However, these compact binaries based on above methods may represent only a small fraction of the overall population when compact object accreting at a sufficiently low rate or in long quiescent periods. Here, radial-velocity modulation in optical spectra are a promising method to uncover unseen compact companion that have a stellar companion (Gu et al. 2019; Liu et al. 2019; Thompson et al. 2019; Yi et al. 2022).

Here we present the first optical spectroscopy and multi-band optical photometry of a single-line binary 2MASS J15274848+3536572 (hereafter J1527), and report that it consists of a K main-sequence and an unseen companion of $M_p = 1.01 \pm 0.08 M_\odot$. We also discuss two possible scenarios that the dark companion of J1527 is a candidate for a white dwarf or a neutron star, respectively. The paper is organized as follows. We describe observations of the source in Section 2, analyse these observations to extract the physical parameters of the source in Section 3. The general discussion of the dark companion in Section 4. Our conclusion are presented in Section 5.

2. OBSERVATIONS

2.1. Optical photometry and open source data

J1527 was also observed with the Nanshan 1m Wide-field Telescope (NOWT) (Bai et al. 2020) of Xinjiang Astronomical Observatory from 2022 April 15 to 2022 April 17 for 3 nights in the B, V and R bands. All the raw images for three bands were overscan correction, bias subtraction and flat fielding using IRAF (Tody 1986, 1993). The optimized aperture photometry was employed using the software SExtractor (Bertin & Arnouts 1996). The resulting differential photometry are relative to a nearby stable reference star in the field, which insensitive to thin clouds or moderate atmospheric variability.

J1527 was classified as a contact eclipsing binaries in the All-Sky Automated Survey (ASAS) and the Catalina Sky surveys (CSS) with period $P = 0.2556686$ d (Drake et al. 2014; Jayasinghe et al. 2019). We obtained sampled light curves from ASAS and CSS, a densely sampled light curve from the SuperWASP, the Transiting Exoplanet Survey Telescope (TESS) and Hungarian Automated Telescope (HAT) (Hartman et al. 2011), which is shown in Figure 1. In addition, it also was observed with GALEX as part of the Medium Imaging Survey with the measured fluxes of $(2.42 \pm 0.34) \times 10^{-13}$ and $(1.25 \pm 0.05) \times 10^{-12} \text{ erg cm}^{-2} \text{ s}^{-1}$ in the far- and near-ultraviolet (FUV and NUV), respectively. In *Gaia* EDR3, the source_id of J 1527 is =1375051479376039040 (Gaia Collaboration et al. 2021). Its EDR3 parallax of $\omega_{\text{EDR3}} = 8.44844 \pm 0.011068 \text{ mas}$ implies a distance of $d = 118.13 \pm 0.86 \text{ pc}$, which is consistent with its *Gaia* DR2 parallax. *Gaia* DR2 also reports a luminosity $L_{\text{Gaia}} = 0.101161 \pm 0.000605 L_\odot$, temperature $T_{\text{eff,Gaia}} = 4047^{+171}_{-109} \text{ K}$, and radius $R_{\text{Gaia}} = 0.65^{+0.03}_{-0.05} R_\odot$ for the star that are consistent with K main-sequence star (Gaia Collaboration et al. 2018).

2.2. Optical spectra

The Large Sky Area Multi-Object fiber Spectroscopic Telescope (LAMOST) is a 4m Schmidt telescope with a 5° field of view, and has become the first spectroscopic survey to collect tens of millions spectra from the universe with

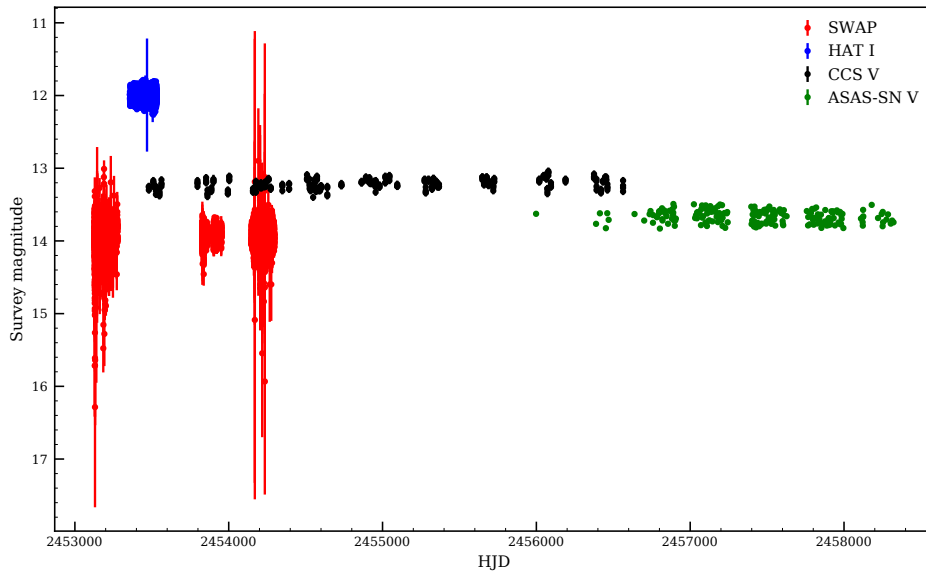


Figure 1. SuperWASP, HATNet, CCS, and ASAS-SN photometry for J1527 from 2004 May 2 to 2018 July 22. No evidence for outbursts appears in the total 5193 d time-span.

both the medium resolution and low resolution modes. The medium resolution observations have $R \sim 7500$ with both a blue and a red arms of a limiting magnitude $G = 15$ mag (Zong et al. 2020). The wavelength coverage of the blue arm is from 495 nm to 535 nm, while from 630 nm to 680 nm for the red arm. The low resolution observation mode has a limiting magnitude as faint as $r \sim 17.8$ mag, with a resolution $R \sim 1800$, and the wavelength range is from 370 nm to 900 nm (Zhao et al. 2012).

Here, we obtained two low-resolution spectra and ten medium-resolution spectra of J1527 from the LAMOST archives data. The low-resolution LAMOST spectra indicate it to be a K type star (Figure 2) with clear signs of the Ca II H&K, Balmer H_α and H_β emission lines, which tells us it is of chromospheric activity. However, the H_α emission shows wider range and a complex morphology including a extra peak emission profile in many observations, which may suggest the presence of an accretion disk. We derived a barycentric velocity of each spectrum through the cross-correlation technique.

2.3. Radio and X-ray observations

We searched for radio pulsations using the FAST (Five-hundred-meter Aperture Spherical radio Telescope). Observations were acquired at 1.4 GHz using the central beam of multibeam receiver. The J1527 was observed for 40 min and 50 min on 2021 October 28 and 2022 September 14, respectively. Using the PRESTO pulsar search suite (Ransom 2001), we excised radio frequency interference and performed an acceleration search to retain sensitivity by setting the z_{max} value to be 200, as well as trial dispersion measures between 0 and 22 pc cm^{-3} . In addition, 1RXS J152748.8+353658 was listed in the ROSAT ALL-Sky Survey Source Catalogue as a faint X-ray source (Voges et al. 1999), with a count rate of $0.0316 \text{ cts s}^{-1}$ in the 0.1-2.4 keV PSPC range. More recently, the RASS was reprocessed by Boller et al. (2016) and the count rate were updated (count rate $0.0342 \pm 0.0122 \text{ cts s}^{-1}$), which is equivalent to observed fluxes of $4.82 \pm 1.72 \times 10^{-13} \text{ erg cm}^{-2} \text{ s}^{-1}$ using the energy to count conversion factor ($\text{ECF} = 1.41 \times 10^{-11} \text{ erg cm}^{-2} \text{ s}^{-1} / \text{count}$) as in Schwöpe et al. (2002).

3. RESULTS

3.1. Properties of the main-sequence K star

We obtained the surface temperatures (T_{eff}) and radius (R) of the K type star by fitting the spectral energy distribution (SED) using the astroARIADNE (Vines & Jenkins 2022). For the SED, we used the photometry from *Gaia* DR2 (G , G_{BP} , and G_{RP}), 2MASS (J , H and K_s), SDSS (r and i), JOHNSON (B and V) and WISE ($W1$ and

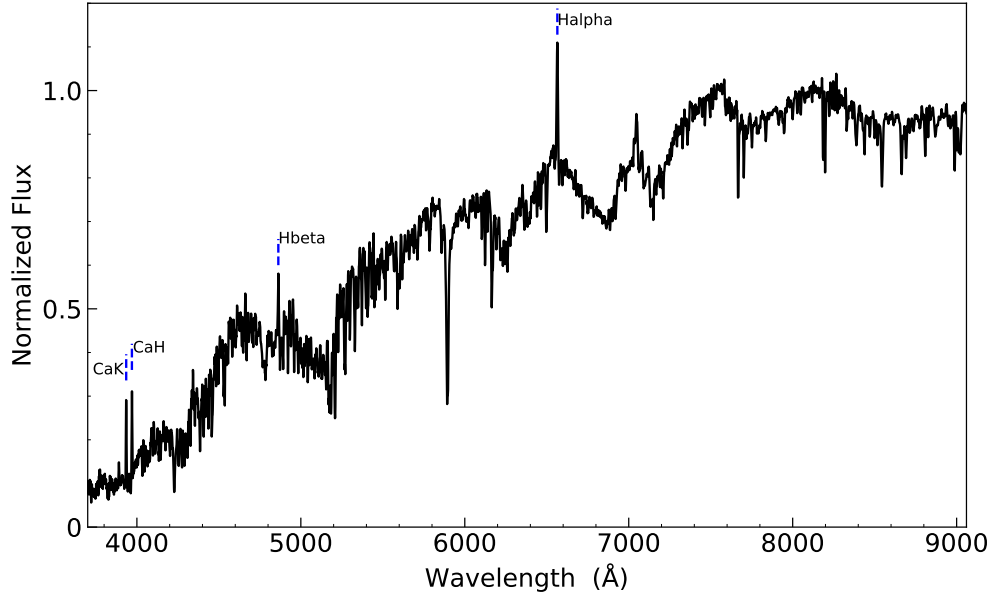


Figure 2. Low-resolution LAMOST spectrum from 2020 January 22, showing the late K spectral type star and the clear Ca II H&K, Balmer H_α and H_β emission line.

W2). We found an excellent fit by using the extinction parameters $A_V = 0$ derived from three-dimensional dust maps of [Green et al. \(2019\)](#), with $T_{\text{eff}} = 3925.02^{+33.70}_{-26.87}$ K and $R = 0.685^{+0.012}_{-0.011} R_\odot$, which are consistent with that of *Gaia* DR2.

Figure 4 shows the variations of the H_α emission line profiles with orbital phase, which corrected to the rest frame of the K star and companion, respectively. We found that the H_α profiles almost peaks directly at or very near the velocity of the K star. This suggests that the H_α emission results from the K-star’s surface. Considering that the H_α emission tracks the orbital motion and the observed Ca II H&K emission in the low-resolution spectra, the H_α emission could be from chromospheric activity as discussed in Section 2.2.

However, the H_α emission profile occasionally shows a broad and complex morphology. Furthermore, the H_α emission presents the other peaked profile in addition to the emission lines of the chromospheric activity ($\phi = 0.195; 0.704; 0.803$). The presence of a broad, double-peaked H_α emission profile has generally been accepted as evidence for an accretion disk in the system ([Wang et al. 2009](#); [Strader et al. 2015](#)). However, the shape of the H_α emission lines from an accretion disk depends on an inclination angle and the choice of power law n and disk base-density ρ_0 ([Silaj et al. 2010](#)). One possible explanation for a broad and complex H_α emission may arise from a combination of an accretion disc around the dark companion and the stellar chromosphere. Here, the extra -peaked H_α emission profile from an accretion disk hard to be identified when the chromosphere of the star is the main contributor to the emission. Overall, we interpret the other peaked H_α emission as evidence of an accretion disk, with rich phenomenology that deserves further study.

3.2. Radial velocities curves

After correcting the observation epochs to Barycentric Julian Date (BJD) on the Barycentric Dynamical Time system, we performed a circular Keplerian model fit to our radial velocity data using the custom Markov chain Monte Carlo sampler TheJoker ([Price-Whelan et al. 2017](#)). Here, we fit the four free parameters for the period P , the ascending node T_0 , systemic velocity γ and the semi-amplitude K . We obtain $P = 0.25566996$ days, $T_0 = 2457091.4790$ days, $K = 172.72^{+0.74}_{-0.73}$ km s $^{-1}$ and $\gamma = -26.14^{+0.68}_{-0.70}$ km s $^{-1}$. We find that the spectroscopic period is basically consistent with the photometric period reported from the ASAS and CSS. The phased radial velocity curve is shown in Figure 5. We used the posterior samples from this fit to derive the mass function $f(M)$

$$f(M) = \frac{PK^3}{2\pi G} = \frac{M_p^3 \sin^3 i}{1 + q} \quad (1)$$

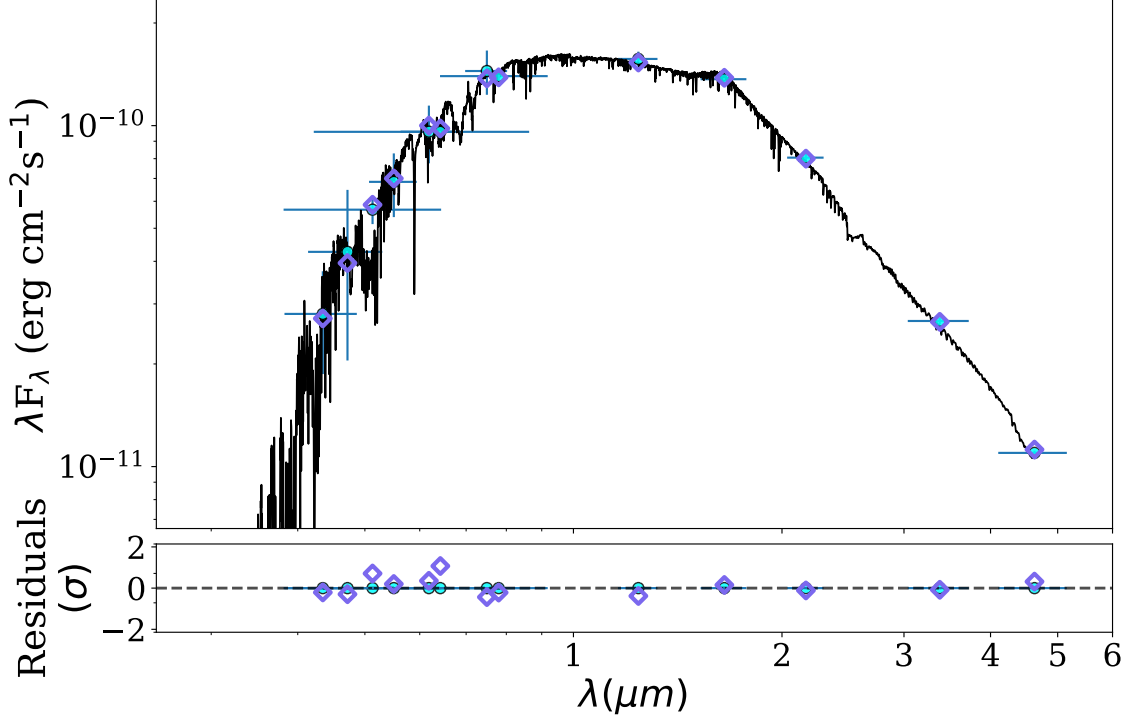


Figure 3. The best-fitting SED model for J1527 after fixing the extinction parameters $A_V = 0$. The black curve is the best-fitting model. The green circles and blue diamonds are the photometric data and the synthetic fluxes from the theoretical spectral, respectively.

for mass ratio q and inclination i . We find $f(M) = 0.135 \pm 0.002 M_\odot$.

3.3. Light-curve modelling

The light curves of J1527 clearly shows a significant ellipsoidal variability with a rather small amplitude. The light curves are asymmetric in the phased light curve of the TESS T-band, showing the fluxes of the two maxima are different, while there are two maxima and one minima in the phased light curve of the B, V, and R-band. This suggest that the star spot patterns evolve with time as the chromospheric activity change. Here, we assume that the visible star filling its Roche lobe given by the evidence for an accretion disk and the accretion disk does not contribute significantly to the optical luminosity of the system due to low X-ray luminosity of the system. Indeed, there are also no evidence for irradiation in the light curve.

To fit the B, V, and R-band light curve, we had to add one spot on the K-star surface with the longitude, latitude, angular radius, and temperature factor as their parameters while it is need two spots for the TESS T-band. We fit the B, V, and R-band light curve and independently fit the TESS T-band using PHOEBE 2.3 (Conroy et al. 2020). Here, we used the option 'distortion method = none' and assume a small ($R = 3 \times 10^{-6} R_\odot$), cold ($T_{\text{eff}} = 300$ K) blackbody, as done in Jayasinghe et al. (2019). We initially performed trial fits to the B, V, and R-band light curves using Nelder-Mead simplex optimization routine. Then, the parameters from trial fit to performed an MCMC run (nwalkers=48, niters=1000, burnin=150) using the emcee (Foreman-Mackey et al. 2019) solver in PHOEBE 2.3. We fit over the following parameters: the binary mass ratio $q = M_K/M_c$, orbital inclination (i), the semimajor axis of the binary (a), the effective temperature (T_{eff}) and one spot of the main-sequence K star in which the parameters of star spot include the longitude, latitude, angular radius, and temperature factor. The results of the fitting are shown in Table 4. We also independently fit the TESS T-band light curve using two star spots and fixed the parameters of q , i , a and $T_{\text{eff,K}}$ that derived from the previous fitting results. The B, V, R, and T-band light curves with best-fitting model from PHOEBE are shown in Figure 6, while the residuals of the model is shown in Figure 7 (See Appendix A). The effective temperature and Roche-lobe radius of the system derived from the PHOEBE model agree well with that obtained from the SED. Combining the modelling of the radial velocity and the PHOEBE model for the ellipsoidal variations, we have enough information to directly determine the masses of the two components in the system. The

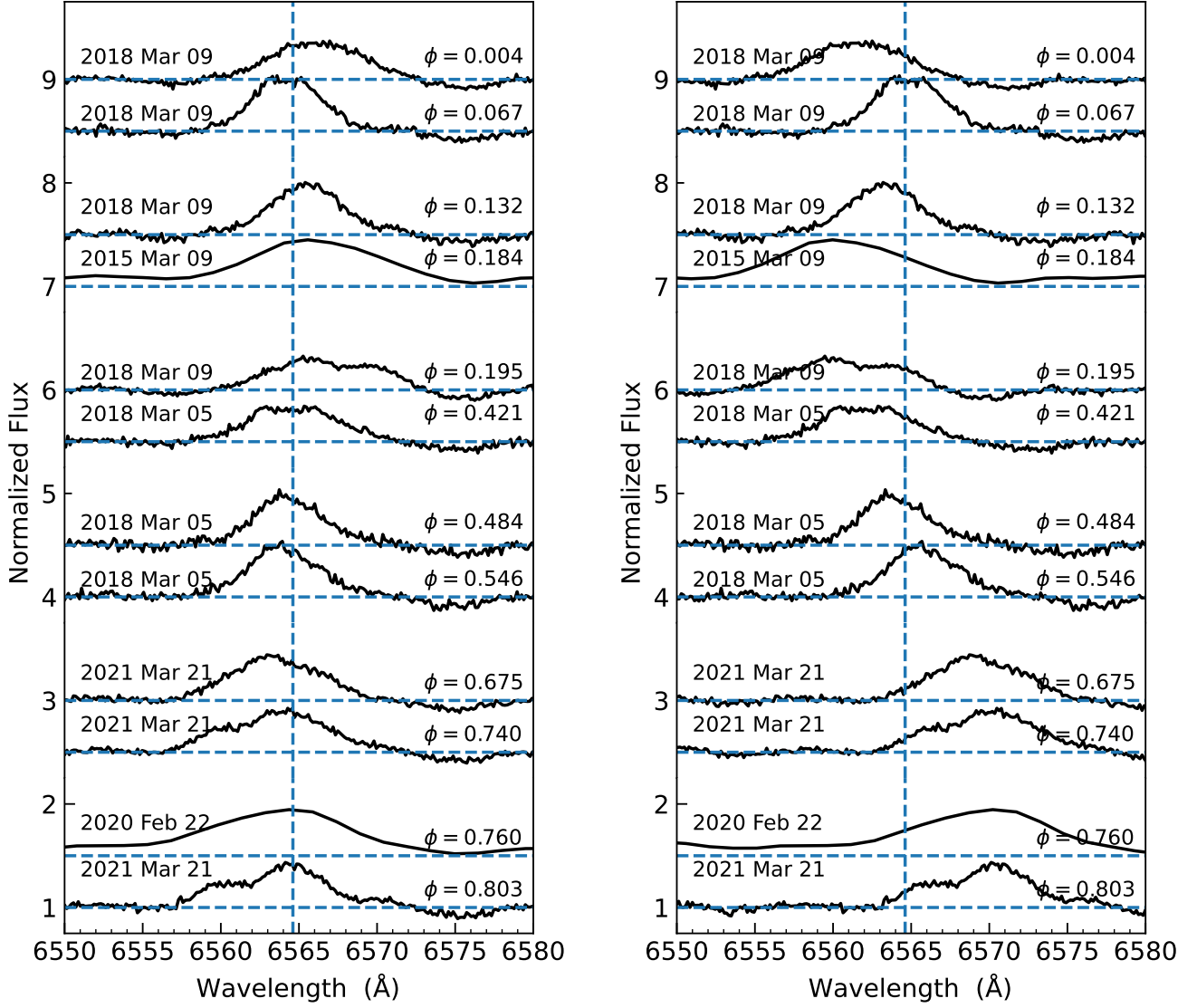


Figure 4. Left: H_{α} emission line profiles as a function of orbital phase in the rest frame of the K-type star. Right: H_{α} emission line profiles in the rest frame of the compact object.

companion mass is

$$M_c = \frac{f(M)(1+q)^2}{\sin^3 i} \quad (2)$$

and from the PHOEBE models, we find that the K main-sequence star has a mass $M_K = 0.59 \pm 0.05 M_{\odot}$ and the companion mass is $M_c = 1.01 \pm 0.08 M_{\odot}$.

3.4. Radio and X-ray detection

The FAST searches have failed to identify a radio pulsar signal from the J1527. In our 40-min searches, we can infer a flux density upper limit of $6 \mu\text{Jy}$ at 1.4 GHz, assuming a minimum detectable signal-to-noise $S/N_{\min} = 10$ and a 20

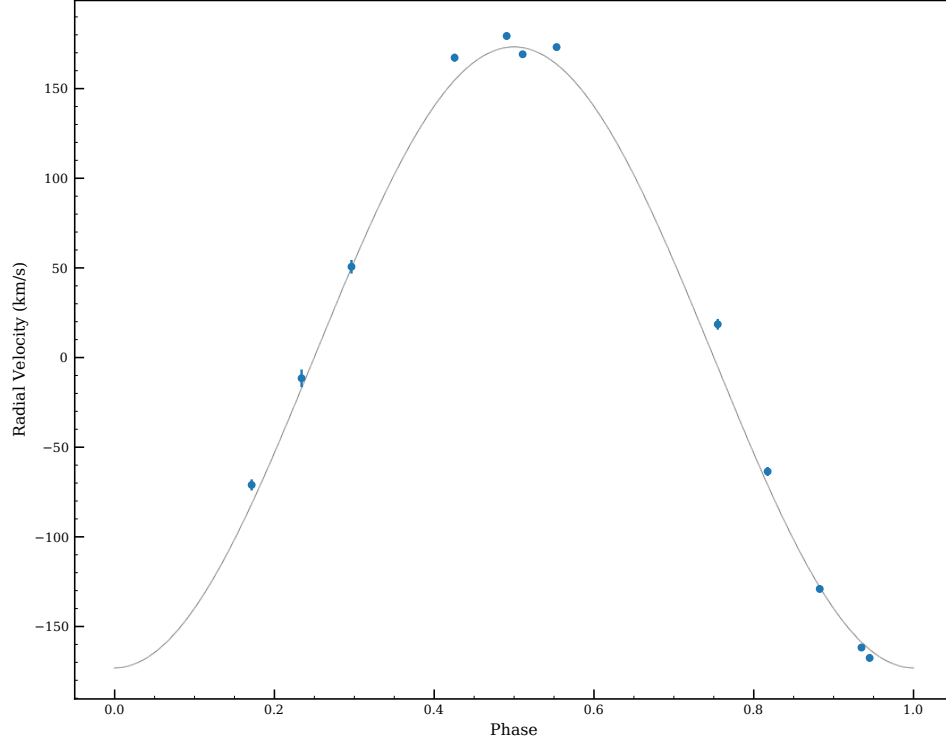


Figure 5. The observed radial velocities for the J1527 as a function of orbital phase obtained in 12 epochs from the LAMOST, with the radial velocities fit is plotted.

Parameter	B, V, and R-band	T-band
P_{orb} (d)	0.25566996 (fixed)	
a (R_{\odot})	$2.123^{+0.048}_{-0.07}$	
i ($^{\circ}$)	$43.94^{+0.33}_{-0.21}$	
T_{eff} (K)	$3920.3^{+2.4}_{-1.7}$	
q	$0.58^{+0.048}_{-0.018}$	
Spot 1 longitude ($^{\circ}$)	$185.48^{+0.28}_{-0.38}$	$307.69^{+0.59}_{-0.35}$
Spot 1 colatitude ($^{\circ}$)	$80.05^{+0.83}_{-1.07}$	$77.07^{+0.9}_{-1.98}$
Spot 1 radius ($^{\circ}$)	$45.56^{+1.69}_{-0.92}$	$53.1^{+2.1}_{-2.2}$
Spot 1 temp. factor	$0.866^{+0.0141}_{-0.0067}$	$0.9187^{+0.0033}_{-0.0044}$
Spot 2 longitude ($^{\circ}$)	—	$159.11^{+1.25}_{-0.82}$
Spot 2 colatitude ($^{\circ}$)	—	$81.25^{+0.17}_{-0.47}$
Spot 2 radius ($^{\circ}$)	—	$24.42^{+0.38}_{-0.17}$
Spot 2 temp. factor	—	$0.6787^{+0.0129}_{-0.0091}$

Table 1. The best-fitting parameter for the B, V, R-band and T-band, respectively

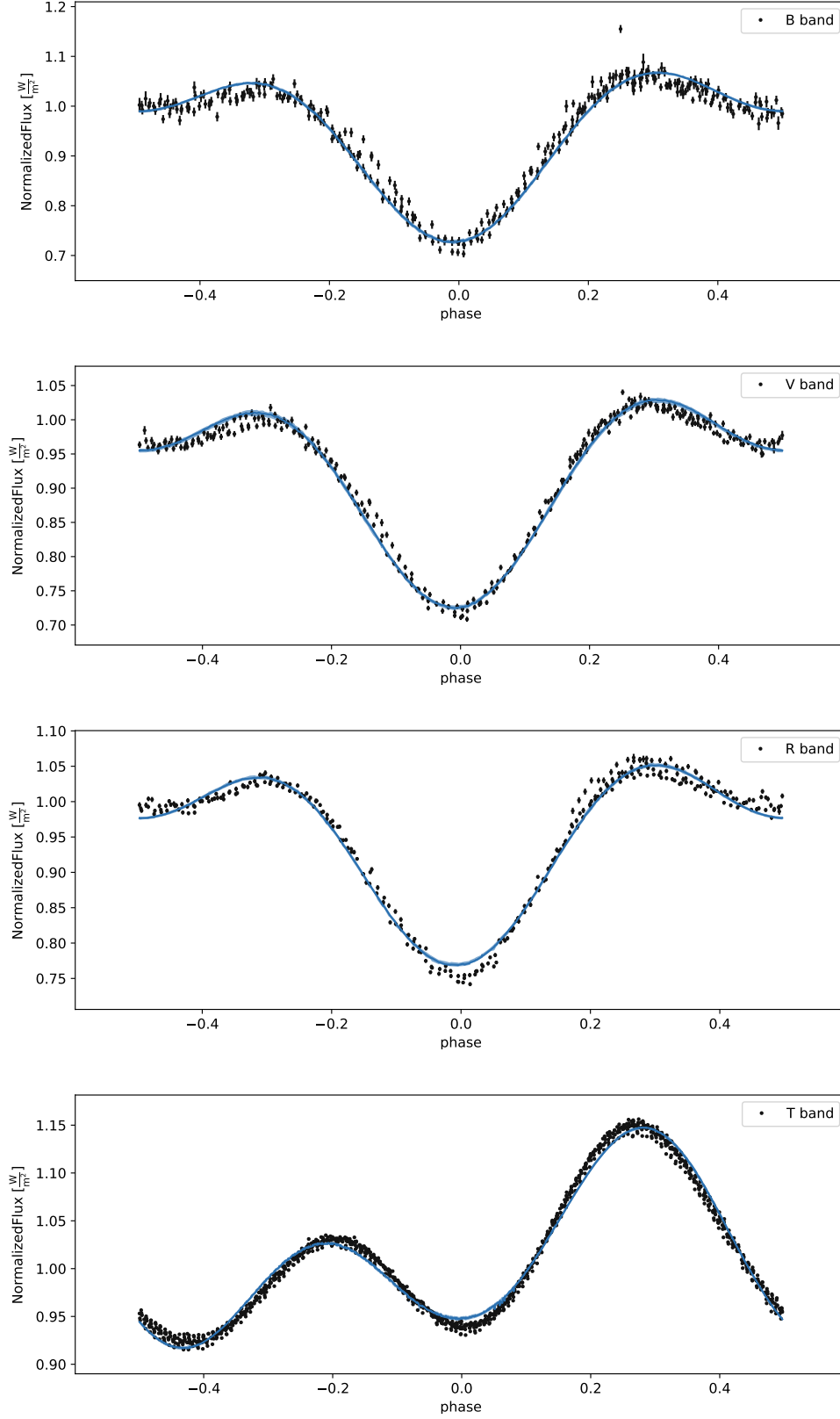


Figure 6. The normalized B, V, R-band and TESS light curves for the J1527 as a function of orbital phase. The blue solid line represents the best-fitting model from PHOEBE.

percent duty cycle. At the Gaia EDR3 distance, we obtain the X-ray luminosities of $(8.12 \pm 3.01) \times 10^{29} \text{ erg s}^{-1}$ in the 0.1-2.4 keV PSPC range of the RASS. The low X-ray luminosity of the system is consistent with the dwarf novae or the chromospherically active RS CVn system (Stelzer et al. 2016). Therefore, the X-ray emission can originate from one of them or mixture of both but also be the compact object.

4. DISCUSSION

4.1. *Is the compact companion a white dwarf in J1527?*

The mass of the compact object ($M_p = 1.01 \pm 0.08 M_\odot$) in J1527, which can be a white dwarf in a CV (an interacting binary system with a white dwarf companion). However, we lay out the arguments that the compact companion in J1527 as a white dwarf will suffer from some troubles. The presence of a broad, extra-peaked H_α emission profile of the J1527 imply the formation of an accretion disc, which helps immediately rule out that the source belong to the polar class. This is because the polar has a strong magnetic field in the range $\sim 10\text{-}300 \text{ MG}$, preventing the formation of an accretion disc (Cropper 1990). In the intermediate polar (IPs), the magnetic field is somewhat smaller and a partial accretion disk is usually present, and the white dwarf does not co-rotate with the orbit (Patterson 1994). However, there are no evidence of any other periodic signal except the orbit period in the optical emission. In addition, the high-ionization emission lines such as He II emission is not clearly present in the LAMOST optical spectra because nearly all magnetic CVs show strong He II emission. Furthermore, the source has an very low X-ray luminosity, which is not consistent with any known X-ray luminosity of the intermediate polar (IPs). Therefore, the source as a candidate for the polar or the intermediate polar looks problematic.

A final discussion concerns the dwarf novae, a class of nonmagnetic CV in which the system undergo outburst to brighten by several magnitudes lasting from days to several weeks. The outbursts are thought to be caused by disc instabilities when the accretion disk reaches a critical density. The J1527 has been detected by the deep GALEX far-and near-ultraviolet (FUV and NUV) and the measured flux of FUV is three times higher than the NUV, and indicating an ultraviolet excess over the flux from the K-type star. In fact, the observed Ca II H&K and H_α emission are present in the low-resolution spectra of J1527 as the common indicators of chromospheric activities, which seemingly suggest that the deep GALEX far-and near-ultraviolet (FUV and NUV) results from stellar chromospheric activity. However, the luminosity of FUV ($4.07 \pm 0.57 \times 10^{29} \text{ erg s}^{-1}$) and NUV ($2.10 \pm 0.09 \times 10^{30} \text{ erg s}^{-1}$) are an order of magnitude higher than the chromospheric luminosity, which is not consistent with the chromospheric activities of the late-type star (Stelzer et al. 2016). Therefore, the FUV and NUV excess may stem from either a white dwarf or an accretion disk. If the FUV and NUV is from a white dwarf, single blackbody model should be able to fit simultaneously the FUV and NUV excess. However, we find that single blackbody model can not fit the FUV and NUV excess, which imply the compact object of J1527 may be not a white dwarf. In addition, if we assume that the NUV excess of the J1527 largely is from the white dwarf, the white dwarf with the effective temperature $T_{\text{eff}} \sim 13194 \text{ K}$ is obtained by fitting ultraviolet emission using single blackbody model with a white dwarf mass of $M_{\text{WD}} = 1.0 M_\odot$ (Figure 7). Then, we can utilize the approximate $T_{\text{eff}} \sim 13194 \text{ K}$ to estimate the accretion rates \dot{M} using the equation of Townsley & Gänsicke (2009):

$$T_{\text{eff}} = 17000(< \dot{M} [M_\odot \text{yr}^{-1}] > / 10^{-10})^{1/4} (M_{\text{wd}} [M_\odot] / 0.9) \text{ K} \quad (3)$$

Using the estimated temperature of white dwarf derived from the far-ultraviolet emission, we can obtain accretion rates $\dot{M} \sim 2.38 \times 10^{-11} M_\odot \text{yr}^{-1}$. The inferred value of the mass-transfer rate is far below the critical accretion rate would be needed to keep the thermal-viscous disk in a stable state at the this orbital period (Dubus et al. 2018), which suggest that the J1527 should exhibit dwarf novae phenomena. However, there are no any evidence for the dwarf nova outburst in our long time-series archives data (See Figure 2). We also note that the fraction of dwarf novae above the period gap can remain in quiescence due to the low accretion rates or large accretion disk (Sokolovsky et al. 2022). If we consider that approximately half of gravitational energy of the accreting gas is liberated through X-rays in the boundary layer, then for a $M_p = 1.01 M_\odot$ white dwarf, the inferred accretion rates $\dot{M} \sim 2.38 \times 10^{-11} M_\odot \text{yr}^{-1}$ implies the X-ray luminosity of $\sim 2.05 \times 10^{32} \text{ erg s}^{-1}$. However, if assume that the observed X-ray luminosity originate entirely from the released gravitational energy of the accreting gas, it is a factor of ~ 100 below the inferred X-ray luminosity.

In summary, we cannot completely rule out that the compact object is a white dwarf in J1527. However, there is no apparent evidence that supports the presence of a white dwarf. Therefore, we consider a scenario that the compact companion is a low-mass neutron star.

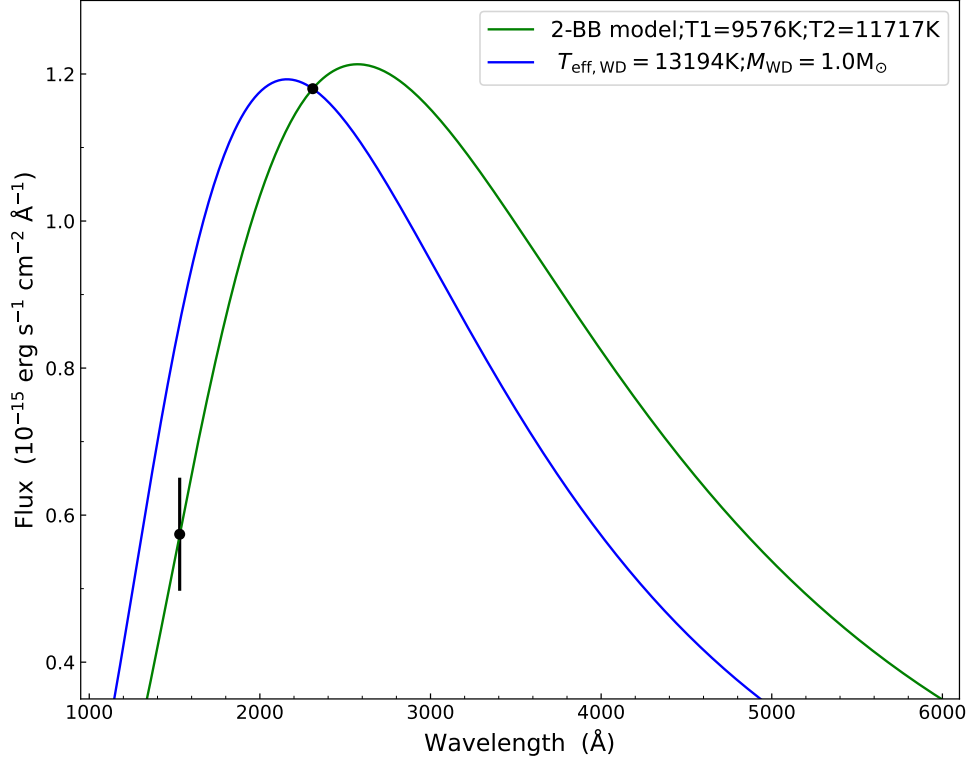


Figure 7. The green line is the best-fit two blackbody model, while the blue line is the result of the NUV flux that fitted by the single blackbody model with a white dwarf of $1.0M_{\odot}$.

4.2. Is the compact companion an “X-ray dim isolated neutron star” in binary J1527?

If the compact companion is not a white dwarf in J1527, then it is a low-mass X-ray binary (LMXB) containing either a neutron star or black hole companion. However, the mass of the compact companion immediately rule out a stellar black hole, which means the most likely scenario is a neutron star. We did not detect the radio pulsations from the J1527 in two observations using FAST, which may suffer from severe scattering and/or absorption due to enshrouding of the system by intra-binary material. The absence of radio pulsations from J1527 seem to the transitional MSPs PSR J1023+0038 that shows the lack of the detection of radio pulsations in the disk state (Stappers et al. 2014). There should be γ ray counterpart due to the interaction between the pulsar wind and the accretion disk if the absence of radio pulsations can be interpreted by the presence of an accretion disk. However, we did not find a possible γ ray counterpart of J1527 from the Fermi-LAT catalog. Therefore, we propose that the dark companion of J1527 is an XDINS-like compact object in binary likely.

The most direct interpretation to account for a low X-ray luminosity is that no or parts of accretion flow reaches the neutron star surface when the magnetospheric radius r_m much larger than the corotation radius r_{co} according to standard accretion theory (Illarionov & Sunyaev 1975). Here, we interpret that the far-and near-ultraviolet (FUV and NUV) come from an accretion disk (Takata et al. 2014), which is consistent with the presence of a broad, additional-peaked H_{α} emission. We use two blackbody to fit the far-and near-ultraviolet with the maximum likelihood estimation. The modeled temperature is $T_1 = 9576$ K and $T_2 = 11717$ K with the corresponding radii $R = 6.3 \times 10^8$ cm. Here, we make a simplified assumption that the corresponding radii R_{BB} is consistent with the magnetospheric radius r_m . The magnetospheric radius is

$$r_m = 1.2 \times 10^9 \mu_{29}^{4/7} \dot{M}_{13}^{-2/7} \left(\frac{M}{M_{\odot}} \right)^{-1/7} = 6.3 \times 10^8 \text{ cm}, \quad (4)$$

where the magnetic moment $\mu = B_p R^3/2 \sim 10^{29} B_{p,11} \text{ Gcm}^3$ and the radius of neutron star $R = 12 \text{ km}$. The observed $L_{\text{bol}} = GMM/2r_m \sim 3 \times 10^{30} \text{ ergs}^{-1}$ derived from the two blackbody model, which gives the disk accretion rate $\dot{M} = 3 \times 10^{13} \text{ g s}^{-1}$. According to equations (4) and the disk accretion rate, we obtain a weak magnetic field of $\sim B_p = 5.6 \times 10^{10} \text{ G}$ for a neutron star. The system is in the propeller regime when the magnetospheric radius larger than the corotation radius ($r_m > r_c$). In this picture, the neutron star with a weak magnetic field must have a spin period $P_{\text{spin}} < 8.58 \text{ s}$, since the corotation radius is

$$r_c = (GMP^2/4\pi^2)^{1/3} = 1.50 \times 10^9 P^{2/3} \text{ cm}. \quad (5)$$

Considering a radio-quiet neutron star with a weak magnetic field, it may locate at the radio pulsar death line because the electric potential of the gap region is too low to generate electron-positron pairs. This also account for the absence of the γ ray in the system. Using the radio pulsar death line $B_p/P^2 = 1.7 \times 10^{11} \text{ G s}^{-2}$ (Bhattacharya et al. 1992), we obtain the spin period of death line $P_{\text{spin}} \sim 0.57 \text{ s}$. Therefore, we estimate the spin period of the neutron star $0.57 \text{ s} \leq P_{\text{spin}} \leq 8.58 \text{ s}$, which also is consistent with the characteristic spin period of the XDINS (Kaplan et al. 2011).

In addition, a neutron star with $M_p \sim 1.00 M_\odot$ will be lightest neutron star, which challenge the paradigm of gravitational-collapse neutron star formation (Lattimer 2012). However, a low-mass limit ($0.9 - 1.1 M_\odot$) is also suggested when considering both thermal and neutrino-trapping effects are large (Goussard et al. 1998; Strobel et al. 1999). More interestingly, one discover that the radionuclide ^{60}Fe signal observed in deep-sea crusts is global, which indicate multiple supernova events during the last ten million years within $\sim 100 \text{ pc}$ of Earth (Wallner et al. 2016; Ertel et al. 2022; Zheng et al. 2022). The XDINS-like compact object with $\sim 118 \text{ pc}$ make it the nearest neutron star, which may suggest the radionuclide ^{60}Fe signal from the deep-sea crusts is associated with its supernova event. Furthermore, we performed a kinematic analysis of J1527's orbit in the Galaxy using the Gaia astrometric solution and the systematic radial-velocity (See Appendix B), which imply that it can pass through our solar neighborhood and is consistent with residing in the Galactic thin disk.

The discovery of compact object in J1527 likely imply that some XDINS-like objects keep in binary when they received low kicks at birth. As a result, there may be lots of XDINS-like stars, either as single or in binary, in the Milky Way since that these neutron stars are dim and close to us. Our finding may hint that XDINS-like compact objects would be born in an alternative channel rather than the standard core-collapse supernova, as discussed about an accretion-induced collapse (AIC) of an ONeMg white dwarf (Taani 2022) for instance.

5. CONCLUSIONS

We identify a K-type star of chromospheric activity in a binary system with dark companion mass of $M_p = 1.01 \pm 0.08 M_\odot$. By modelling the multi-band light curve with PHOEBE, we derive an inclination of $43.94_{-0.21}^{+0.33}^\circ$, a mass ratio of $0.58_{-0.018}^{+0.048}$, and a K-type star's mass of $0.59 \pm 0.05 M_\odot$ using constraints on the RV, orbital period, and stellar temperature. The low-resolution LAMOST spectrum uncover the H_α emission of wider range and the other peak emission, which suggest the presence of an accretion disk. Here, the dark companion mass of $M_p = 1.01 \pm 0.08 M_\odot$ is either a white dwarf or a neutron star. However, the system shows some characteristics seem to contradict a cataclysmic variable due to lack of any observed outburst in 5193 d time-series of optical observation. Therefore, we discuss the other possible that the unseen compact companion as a low-mass neutron star. If the dark companion is confirmed as a neutron star, it will be nearest and lightest neutron star yet. These features, together with X-ray dim and radio-quiet, are similar to that of XDINSs, and we thus suggest the J1527 binary may host an XDINS-like compact object.

To determine the nature of the compact object and understand this unique system, further multi-band observation are necessary. Especially, the observation of the Hubble Space Telescope spectroscopy will determine whether the compact object is a white dwarf and the X-ray observation may also address the nature of the compact object. In addition, searching for radio pulsations or the radio jet from the J1527 system would nail it down as a neutron star.

ACKNOWLEDGMENTS

We appreciate Jianning Fu, Kejia Lee, Bojun Wang, Chunyang Cao and Jianping Xiong for their helpful comments and suggestions. Guoshoujing Telescope (the Large Sky Area Multi-Object Fiber Spectroscopic Telescope, LAMOST) is a National Major Scientific Project built by the Chinese Academy of Sciences. Funding for the project has been provided by the National Development and Reform Commission. LAMOST is operated and managed by the National Astronomical Observatories, Chinese Academy of Sciences. FAST is a Chinese national mega-science facility, operated by the National Astronomical Observatories, Chinese Academy of Sciences. This paper makes use of data from the first public release of the WASP data (Butters et al. 2010) as provided by the WASP consortium and services at the NASA Exoplanet Archive, which is operated by the California Institute of Technology, under contract with the National Aeronautics and Space Administration under the Exoplanet Exploration Program. This paper includes data collected with the TESS mission, obtained from the MAST data archive at the Space Telescope Science Institute (STScI). Funding for the TESS mission is provided by the NASA Explorer Program. STScI is operated by the Association of Universities for Research in Astronomy, Inc., under NASA contract NAS 5-26555. We acknowledge the use of the public data from the ASAS, CRST and HATNet. This research has made use of the SIMBAD database, operated at CDS, Strasbourg, France. This work was supported by the National SKA Program of China (2020SKA0120100), the national natural science foundation of china (12090040, 12090044, 11833006), and the Strategic Priority Research Program of CAS (XDB23010200).

REFERENCES

- Boller, T., Freyberg, M. J., Trümper, J., et al. 2016, *A&A*, 588, A103. doi:10.1051/0004-6361/201525648
- Bai, C.-H., Feng, G.-J., Zhang, X., et al. 2020, *Research in Astronomy and Astrophysics*, 20, 211. doi:10.1088/1674-4527/20/12/211
- Bertin, E. & Arnouts, S. 1996, *A&AS*, 117, 393. doi:10.1051/aas:1996164
- Butters, O. W., West, R. G., Anderson, D. R., et al. 2010, *A&A*, 520, L10. doi:10.1051/0004-6361/201015655
- Bhattacharya, D., Wijers, R. A. M. J., Hartman, J. W., et al. 1992, *A&A*, 254, 198
- Cropper, M. 1990, *SSRv*, 54, 195. doi:10.1007/BF00177799
- Conroy, K. E., Kochoska, A., Hey, D., et al. 2020, *ApJS*, 250, 34. doi:10.3847/1538-4365/abb4e2
- Drake, A. J., Graham, M. J., Djorgovski, S. G., et al. 2014, *ApJS*, 213, 9. doi:10.1088/0067-0049/213/1/9
- Dubus, G., Otulakowska-Hypka, M., & Lasota, J.-P. 2018, *A&A*, 617, A26. doi:10.1051/0004-6361/201833372
- Ertel, A. F., Fry, B. J., Fields, B. D., et al. 2022, *arXiv:2206.06464*
- Foreman-Mackey, D., Farr, W., Sinha, M., et al. 2019, *The Journal of Open Source Software*, 4, 1864. doi:10.21105/joss.01864
- Fryer, C. L., Belczynski, K., Wiktorowicz, G., et al. 2012, *ApJ*, 749, 91. doi:10.1088/0004-637X/749/1/91
- Goussard, J.-O., Haensel, P., & Zdunik, J. L. 1998, *A&A*, 330, 1005
- Green, G. M., Schlafly, E., Zucker, C., et al. 2019, *ApJ*, 887, 93. doi:10.3847/1538-4357/ab5362
- Gu, W.-M., Mu, H.-J., Fu, J.-B., et al. 2019, *ApJL*, 872, L20. doi:10.3847/2041-8213/ab04f0
- Gaia Collaboration, Brown, A. G. A., Vallenari, A., et al. 2018, *A&A*, 616, A1. doi:10.1051/0004-6361/201833051
- Gaia Collaboration, Brown, A. G. A., Vallenari, A., et al. 2021, *A&A*, 649, A1. doi:10.1051/0004-6361/202039657
- Haberl, F. 2007, *Ap&SS*, 308, 181. doi:10.1007/s10509-007-9342-x
- Hartman, J. D., Bakos, G. Á., Noyes, R. W., et al. 2011, *AJ*, 141, 166. doi:10.1088/0004-6256/141/5/166
- Ho, W. C. G., Kaplan, D. L., Chang, P., et al. 2007, *MNRAS*, 375, 821. doi:10.1111/j.1365-2966.2006.11376.x
- Illarionov, A. F., & Sunyaev, R. A. 1975, *A&A*, 39, 185
- Lattimer, J. M. 2012, *Annual Review of Nuclear and Particle Science*, 62, 485. doi:10.1146/annurev-nucl-102711-095018
- Jayasinghe, T., Stanek, K. Z., Thompson, T. A., et al. 2021, *MNRAS*, 504, 2577. doi:10.1093/mnras/stab907
- Jayasinghe, T., Stanek, K. Z., Kochanek, C. S., et al. 2019, *MNRAS*, 486, 1907. doi:10.1093/mnras/stz844
- Kaplan, D. L., Kamble, A., van Kerkwijk, M. H., et al. 2011, *ApJ*, 736, 117. doi:10.1088/0004-637X/736/2/117
- Kaspi, V. M. 2010, *Proceedings of the National Academy of Science*, 107, 7147. doi:10.1073/pnas.1000812107
- Langer, N. 2012, *ARA&A*, 50, 107. doi:10.1146/annurev-astro-081811-125534
- Liu, J., Zhang, H., Howard, A. W., et al. 2019, *Nature*, 575, 618. doi:10.1038/s41586-019-1766-2
- Mukai, K. 2017, *PASP*, 129, 062001. doi:10.1088/1538-3873/aa6736

- Pires, A. M., Motch, C., & Janot-Pacheco, E. 2009, *A&A*, 504, 185. doi:10.1051/0004-6361/200912180
- Pires, A. M., Motch, C., Turolla, R., et al. 2015, *A&A*, 583, A117. doi:10.1051/0004-6361/201526436
- Price-Whelan, A. M., Hogg, D. W., Foreman-Mackey, D., et al. 2017, *ApJ*, 837, 20. doi:10.3847/1538-4357/aa5e50
- Price-Whelan, A. M. 2017, *The Journal of Open Source Software*, 2, 388. doi:10.21105/joss.00388
- Patterson, J. 1994, *PASP*, 106, 209. doi:10.1086/133375
- Ransom, S. M. 2001, Ph.D. Thesis
- Ramsay, G., Wood, M. A., Cannizzo, J. K., et al. 2017, *MNRAS*, 469, 950. doi:10.1093/mnras/stx859
- Rigoselli, M., Mereghetti, S., & Tresoldi, C. 2022, *MNRAS*, 509, 1217. doi:10.1093/mnras/stab2974
- Strobel, K., Schaab, C., & Weigel, M. K. 1999, *A&A*, 350, 497
- Silaj, J., Jones, C. E., Tycner, C., et al. 2010, *ApJS*, 187, 228. doi:10.1088/0067-0049/187/1/228
- Stappers, B. W., Archibald, A. M., Hessels, J. W. T., et al. 2014, *ApJ*, 790, 39. doi:10.1088/0004-637X/790/1/39
- Sokolovsky, K. V., Strader, J., Swihart, S. J., et al. 2022, *ApJ*, 934, 142. doi:10.3847/1538-4357/ac7b25
- Schwope, A. D., Brunner, H., Buckley, D., et al. 2002, *A&A*, 396, 895. doi:10.1051/0004-6361:20021386
- Strader, J., Chomiuk, L., Cheung, C. C., et al. 2015, *ApJL*, 804, L12. doi:10.1088/2041-8205/804/1/L12
- Stelzer, B., Damasso, M., Scholz, A., et al. 2016, *MNRAS*, 463, 1844. doi:10.1093/mnras/stw1936
- Tody, D. 1986, *Proc. SPIE*, 627, 733. doi:10.1117/12.968154
- Tody, D. 1993, *Astronomical Data Analysis Software and Systems II*, 52, 173
- Townsley, D. M. & Gänsicke, B. T. 2009, *ApJ*, 693, 1007. doi:10.1088/0004-637X/693/1/1007
- Thompson, T. A., Kochanek, C. S., Stanek, K. Z., et al. 2019, *Science*, 366, 637. doi:10.1126/science.aau4005
- Takata, J., Li, K. L., Leung, G. C. K., et al. 2014, *ApJ*, 785, 131. doi:10.1088/0004-637X/785/2/131
- Taani, A. 2022, arXiv:2210.08125
- Vines, J. I. & Jenkins, J. S. 2022, *MNRAS*, 513, 2719. doi:10.1093/mnras/stac956
- Voges, W., Aschenbach, B., Boller, T., et al. 1996, *IAUC*, 6420
- Voges, W., Aschenbach, B., Boller, T., et al. 1999, *A&A*, 349, 389
- Wang, J., Fu, J., Niu, H., et al. 2021, *MNRAS*, 504, 4302. doi:10.1093/mnras/stab1219
- Wang, Z., Archibald, A. M., Thorstensen, J. R., et al. 2009, *ApJ*, 703, 2017. doi:10.1088/0004-637X/703/2/2017
- Wallner, A., Feige, J., Kinoshita, N., et al. 2016, *Nature*, 532, 69. doi:10.1038/nature17196
- Wang, W., Lu, J., Tong, H., et al. 2017, *ApJ*, 837, 81. doi:10.3847/1538-4357/aa5e52
- Wang, W.-Y., Feng, Y., Lai, X.-Y., et al. 2018, *Research in Astronomy and Astrophysics*, 18, 082. doi:10.1088/1674-4527/18/7/82
- Woosley, S. E., Sukhbold, T., & Janka, H.-T. 2020, *ApJ*, 896, 56. doi:10.3847/1538-4357/ab8cc1
- Yi, T., Gu, W.-M., Zhang, Z.-X., et al. 2022, *Nature Astronomy*, 6, 1203. doi:10.1038/s41550-022-01766-0
- Zhao, G., Zhao, Y.-H., Chu, Y.-Q., et al. 2012, *Research in Astronomy and Astrophysics*, 12, 723. doi:10.1088/1674-4527/12/7/002
- Zong, W., Fu, J.-N., De Cat, P., et al. 2020, *ApJS*, 251, 15. doi:10.3847/1538-4365/abbb2d
- Zheng, L.-L., Sun, M., Gu, W.-M., et al. 2022, arXiv:2210.04685

APPENDIX

A. SHORT TIME-SCALE VARIABILITY IN THE RESIDUALS

There are extra variability on the time-scales of days or longer in the residuals of the B, V, and R bands and TESS T-band light curves after subtracting the best model. In addition, the residuals exhibit similar characteristics in the light curves. We searched for additional variability on the time-scale of days in the TESS T-band light curve and find no evidence of variability on any other period. Further, there is no periodic signal after pre-whitening the data on the main period using higher cadence observation for B, V, and R band (Ramsay et al. 2017). Therefore, the residuals of the light curve show quasi-sinusoidal signals, which may be induced by the some small star spots on the K star's surface (Wang et al. 2021).

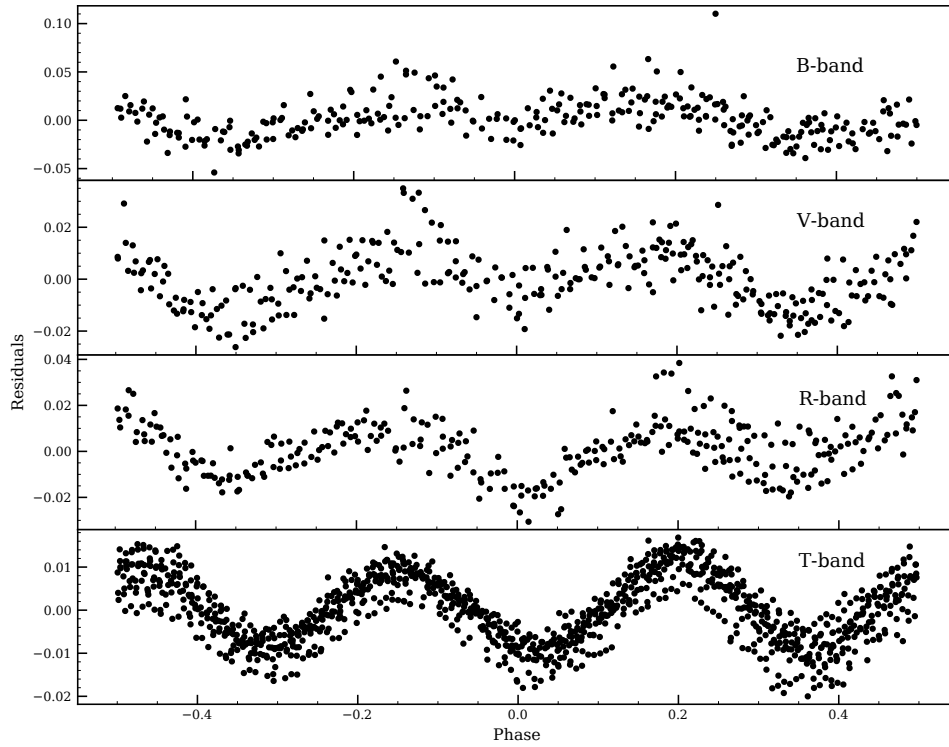


Figure 8. The light curve residuals for multi-band (B,V,R and T) after the PHOEBE model is subtracted.

B. THE KINEMATIC ANALYSIS OF J1527

We use the Gala code to compute its trajectory around the Milky Way over 50 Myr (Price-Whelan 2017), using the Milky Way potential. Here, we use the parallax and proper motion reported by the Gaia, and the systematic radial velocity fitted by our radial velocity data. This suggests that the J1527 reside in the Galactic thin disk and the system pass though our solar neighborhood (within ~ 100 pc) in the past 5Myr.

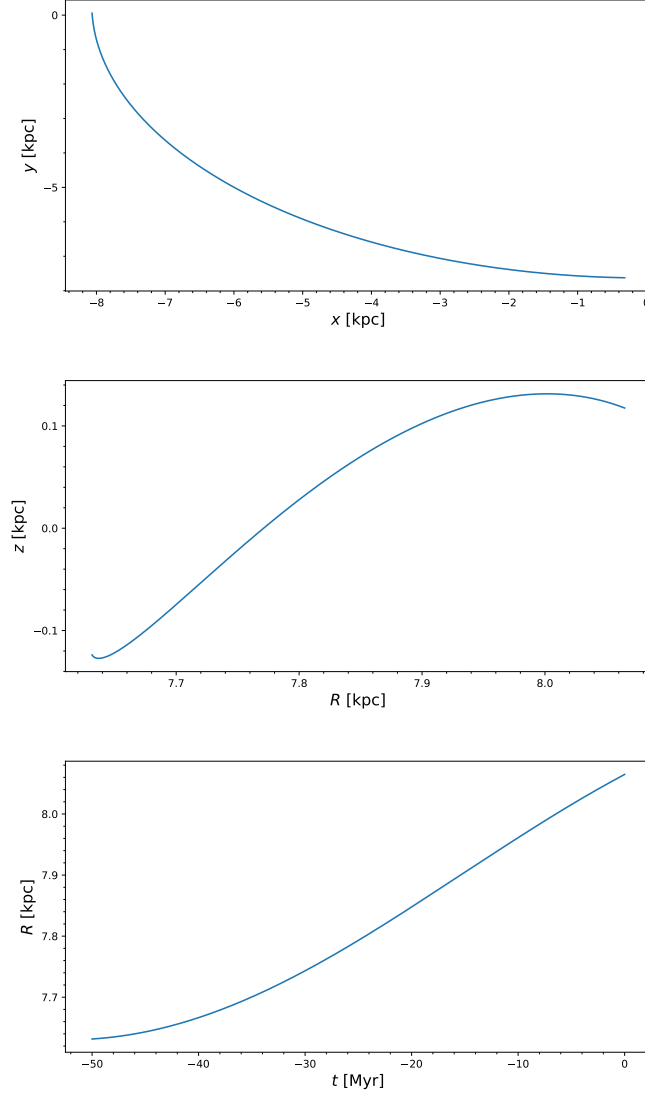


Figure 9. A set of panels shows the trajectory of J1527 around the Milky Way integrated backwards from present day for 50 Myr.